

Quantum process tomography of adiabatic and superadiabatic stimulated Raman passage

Shruti Dogra and Gheorghe Sorin Paraoanu

(Dated: 24 November 2021)

Abstract. Quantum control methods for three-level systems have become recently an important direction of research in quantum information science and technology. Here we present numerical simulations using realistic experimental parameters for quantum process tomography in STIRAP (stimulated Raman adiabatic passage) and saSTIRAP (superadiabatic STIRAP). Specifically, we identify a suitable basis in the operator space as the identity operator together with the 8 Gell-Mann operators, and we calculate the corresponding process matrices, which have $9 \times 9 = 81$ elements. We discuss these results for the ideal decoherence-free case, as well as for the experimentally-relevant case with decoherence included.

INTRODUCTION

With rapidly advancing experimental approach to quantum computation and quantum information [1], and especially with newly emerging era of cloud-based experimental quantum computing platforms [2, 3], the running of algorithms on few-qubits processors has become widely available [4, 5, 6, 7, 8, 9, 10, 11, 12]. At the core of these developments are key advancements in improving the fidelity of quantum gates, which require their precise characterization by quantum tomography. Quantum process tomography (QPT) is a method to characterize an arbitrary quantum operation by operating that process on a set of known test states forming a complete basis [13]. Despite being quite demanding in terms of resources, QPT is essential in quantum computing for specifying the accuracy of implementation of quantum gates. There have been several theoretical proposals as well as experimental demonstrations to obtain quantum process tomography [14, 15, 16] and also to reduce the resources [17, 18, 19, 20]. So far, most of the implementations aim at characterizing quantum processes in multi-qubit systems. Here we work out process tomography for a three-level system (qutrit). Multilevel processes provide an efficient way to quantum computing tasks [21] and they are directly relevant for quantum simulations of many-body systems [22, 23]. Other possible applications in the field of circuit QED concern operations via dissipative microwave links [24], multilevel metrology [25, 26], the characterization of qutrit-based quantum computing architectures [27], and the study of the ultrastrong coupling [28].

Here we show how to implement quantum process tomography for a three-level system (qutrit) undergoing adiabatic and superadiabatic processes. Adiabatic processes are an important component of the control toolbox available in quantum physics. In three-level systems, a paradigmatic transfer process is STIRAP (stimulated Raman adiabatic passage) [29], which has been demonstrated with a superconducting circuit [30]. The superadiabatic STIRAP (saSTIRAP) is a process whereby the standard STIRAP is augmented by a counterdiabatic Hamiltonian, which has the role of keeping the system in the dark state and which is obtained by reverse Hamiltonian engineering [31]. This process has also been demonstrated experimentally [32]. Although developed as a way to transfer population, STIRAP and saSTIRAP can also assist in the realization of certain quantum gates [33] and can be applied to superpositions [34]. Recently a geometrical picture of these processes has been developed, based on the Majorana star representation [35].

QUANTUM PROCESS TOMOGRAPHY FOR QUTRITS

Introduction to quantum process tomography Let us consider a d -dimensional quantum system undergoing a process ε which takes an arbitrary state: $\rho \rightarrow \varepsilon(\rho)$. This, using the operator sum representation [1, 36], may be written as

$$\varepsilon(\rho) = \sum_i E_i \rho E_i^\dagger, \quad (1)$$

such that $E_i = \sum e_{im} \tilde{E}_m$, where \tilde{E}_m form a complete basis in d^2 -dimensional operator space and e_{im} are the complex coefficients. We have

$$\varepsilon(\rho) = \sum_{m,n} \tilde{E}_m \rho \tilde{E}_n^\dagger \chi_{mn}, \quad (2)$$

where $\chi_{mn} = \sum_i e_{im} e_{in}^*$. χ_{mn} is a complex positive Hermitian matrix that characterizes the process ε for a fixed set of basis operators: $\{\tilde{E}_m\}$. The aim is to obtain the process matrix χ , but the complex coefficients e_{im} s are not directly accessible. In practical situations however, the more accessible entity is the state of the system, which can be obtained using standard procedures of quantum state tomography (QST) [1, 37]. In order to characterize this process via QST-based alternative approach, the process ε is made to operate on d^2 different linearly independent matrices (ρ_i , $i \in [1, d^2]$), which form a complete basis to represent a quantum state ρ . The resultant states are obtained as

$$\varepsilon(\rho_j) = \sum_k \lambda_{jk} \rho_k, \quad (3)$$

where the coefficients λ_{jk} can be obtained from the QST of respective states $\varepsilon(\rho_j)$. Exploiting the equivalence of the two approaches in Eqns. 2 and 3 for a state ρ_j , we obtain

$$\varepsilon(\rho_j) = \sum_{m,n} \tilde{E}_m \rho_j \tilde{E}_n^\dagger \chi_{mn}, = \sum_k \lambda_{jk} \rho_k \quad (4)$$

$$\text{or} \quad \sum_k \sum_{m,n} \beta_{jk}^{mn} \chi_{mn} \rho_k = \sum_k \lambda_{jk} \rho_k, \quad (5)$$

where $\tilde{E}_m \rho_j \tilde{E}_n^\dagger = \sum_k \beta_{jk}^{mn} \rho_k$. Linear independence of ρ_k s imply that the respective coefficients are to be equated, such that

$$\beta \chi = \lambda \quad \implies \quad \chi = \beta^{-1} \lambda, \quad (6)$$

where χ and λ are d^4 -dimensional vectors, and β is $d^4 \times d^4$ -dimensional invertible matrix with rows labelled by jk and columns by mn [1]. The $d^4 \times 1$ dimensional χ thus obtained is reshuffled to obtain the $d^2 \times d^2$ dimensional process matrix, which uniquely represents the desired process ε for a fixed basis.

The case of qutrits We perform the quantum process tomography for the case of a qutrit, which is a three-level quantum system ($d = 3$). A set of nine matrices, which form a complete basis to represent an arbitrary quantum state in 3×3 -dimensional operator space is $|p\rangle\langle q|$, where $p, q = 0, 1, 2$, which consist of three Hermitian and six non-Hermitian matrices. The procedure for QPT as described earlier is also valid for the non-Hermitian basis, as being used here. For the real situations such as experiments, these non-Hermitian matrices can be realized as a linear combination of Hermitian density operators. The basis set to represent the \tilde{E}_m 's is chosen to be a 3×3 identity operator ($\tilde{E}_1 = \mathbb{I}$) and the eight Gell Mann matrices ($\tilde{E}_{i+1} = \Lambda_i$, $i \in [1, 8]$). The Gell-Mann lambda matrices are a set of 8 matrices that form a representation of the generators of the Lie algebra associated with the group SU(3). They are defined as

$$\begin{aligned} \Lambda_1 &= \begin{pmatrix} 0 & 1 & 0 \\ 1 & 0 & 0 \\ 0 & 0 & 0 \end{pmatrix}, \Lambda_3 = \begin{pmatrix} 1 & 0 & 0 \\ 0 & -1 & 0 \\ 0 & 0 & 0 \end{pmatrix}, \Lambda_5 = \begin{pmatrix} 0 & 0 & -i \\ 0 & 0 & 0 \\ i & 0 & 0 \end{pmatrix}, \Lambda_7 = \begin{pmatrix} 0 & 0 & 0 \\ 0 & 0 & -i \\ 0 & i & 0 \end{pmatrix}, \\ \Lambda_2 &= \begin{pmatrix} 0 & -i & 0 \\ i & 0 & 0 \\ 0 & 0 & 0 \end{pmatrix}, \Lambda_4 = \begin{pmatrix} 0 & 0 & 1 \\ 0 & 0 & 0 \\ 1 & 0 & 0 \end{pmatrix}, \Lambda_6 = \begin{pmatrix} 0 & 0 & 0 \\ 0 & 0 & 1 \\ 0 & 1 & 0 \end{pmatrix}, \Lambda_8 = \frac{1}{\sqrt{3}} \begin{pmatrix} 1 & 0 & 0 \\ 0 & 1 & 0 \\ 0 & 0 & -2 \end{pmatrix}. \end{aligned} \quad (7)$$

Together with the identity matrix $\mathbb{I}_{3 \times 3}$, these matrices can be used to generate any unitary transformations of a qutrit. In order to characterize an arbitrary process ε in a qutrit, we simulate the qutrit in nine different initial states $|p\rangle\langle q|$. Corresponding to each of these states, the qutrit is then allowed to undergo the same process ε . At the end of which, respective final states are obtained via quantum state tomography. These nine final states contribute 81 complex elements, which form 81×1 -dimensional vector λ . The 81×81 -dimensional β results from the combinations of \tilde{E}_m s, finally giving rise to the process matrix χ .

Evaluating a process matrix is of particular importance in experimental situations in order to determine how different is the actual quantum process with decoherence from the intended operation. It is also quite interesting to perform QPT in case of non-trivial evolutions such as with time dependent Hamiltonians ($H(t)$ and/or $[H(t), H(t')] \neq 0$). QPT also helps to strengthen the understanding of various decoherence models. We obtain these process matrices for the case of widely applicable counter-intuitive STIRAP and saSTIRAP processes in a qutrit.

QPT OF STIRAP AND saSTIRAP

Stimulated Adiabatic Raman Passage (STIRAP) ensures the precise population transfer from one quantum state to another [38]. Considering a three-level quantum system with basis states $\{|0\rangle, |1\rangle, |2\rangle\}$, the STIRAP process is exploited here to transfer the population from ground state ($|0\rangle$) to the second excited state ($|2\rangle$). In the light of selection rules that forbid a direct $|0\rangle \rightarrow |2\rangle$ transfer, this process turns out to be quite useful. STIRAP realizes an adiabatic evolution of the system initialized in state $|0\rangle$ to final state $|2\rangle$ using two Gaussian drives Ω_{01} and Ω_{12} acting in a counter-intuitive temporal order. During the evolution, the system at any time t is in instantaneous eigenstate ($|D\rangle = \cos\Theta|0\rangle - \sin\Theta|2\rangle$) of the STIRAP Hamiltonian, where $|D\rangle$ is called the dark state and $\Theta = \tan^{-1}(\Omega_{01}(t)/\Omega_{12}(t))$ is the mixing angle. The effective STIRAP Hamiltonian [30] is obtained by applying the rotating-wave approximation (RWA)

$$H_0 = \frac{\hbar}{2}\Omega_{01}(t) [\cos(\phi_{01})\Lambda_1 + \sin(\phi_{01})\Lambda_2] + \frac{\hbar}{2}\Omega_{12}(t) [\cos(\phi_{12})\Lambda_6 + \sin(\phi_{12})\Lambda_7] - \frac{\hbar}{2} \left[\delta_{01}\Lambda_3 + \frac{\delta_{01} + 2\delta_{12}}{\sqrt{3}}\Lambda_8 - \frac{2\delta_{01} + \delta_{12}}{3}\mathbb{I}_3 \right], \quad (8)$$

where $0-1$ and $1-2$ drives have Gaussian envelopes with standard deviation σ and relative separation t_s , given by

$$\Omega_{01}(t) = \Omega_{01}e^{-t^2/2\sigma^2} \quad \text{and} \quad \Omega_{12}(t) = \Omega_{12}e^{-(t-t_s)^2/2\sigma^2},$$

with phases ϕ_{01} and ϕ_{12} respectively. These microwave fields may be slightly detuned from the respective transmon transition frequencies ω_{01} and ω_{12} by δ_{01} and δ_{12} respectively.

Adiabatic processes are demanding in terms of time, which is not always affordable in real situations. The superadiabatic STIRAP is a protocol that offers a shortcut to the STIRAP process, in order to have a precise population transfer in experimentally feasible time scales [31]. The superadiabatic STIRAP is obtained by adding a counterdiabatic term,

$$H_{cd} = -\frac{\hbar}{2}\Omega_{02}(t) [\cos(\phi_{02})\Lambda_4 + \sin(\phi_{02})\Lambda_5], \quad (9)$$

which is experimentally realized by a two-photon process [39]. Here we obtain an effective Rabi coupling with absolute value $\Omega_{02}(t) = 2\Theta(t)$ and complex phase ϕ_{02} ; also it is convenient to use the notation $\phi_{02} = -\phi_{20}$. The counteradiabatic condition also implies $\phi_{01} + \phi_{12} + \phi_{20} = -\pi/2$. Based on an analysis of gauge invariance [32, 39], we can take for simplicity $\phi_{01} = \phi_{12} = 0$. Note that for $\phi_{02} = \pi/2$, the counterdiabatic Hamiltonian H_{cd} yields the evolution $\exp\left[i\hbar\Lambda_5 \int_{t_i}^t \dot{\Theta}(t) dt\right]$.

This is experimentally realized by a two-photon resonance pulse [39],

$$H_{2ph} = \frac{\hbar}{2}\Omega_{2ph} [\cos(\phi_{2ph} - \Delta t)\Lambda_1 - \sin(\phi_{2ph} - \Delta t)\Lambda_2] + \frac{\hbar}{\sqrt{2}}\Omega_{2ph} [\cos(\phi_{2ph} + \Delta t)\Lambda_6 - \sin(\phi_{2ph} + \Delta t)\Lambda_7]. \quad (10)$$

with the amplitude of the drive $|\Omega_{2ph}| = \sqrt{\sqrt{2}\Delta\Omega_{02}}$ and phase $\phi_{2ph} = -(\phi_{20} + \pi)/2$, which simultaneously drives the $|0\rangle \rightarrow |1\rangle$ and $|1\rangle \rightarrow |2\rangle$ transitions with detunings $\mp\Delta$ respectively, where $\Delta = (\omega_1 - \omega_2)/2$. The saSTIRAP Hamiltonian is thus given by

$$H_{saSTIRAP} = H_0 + H_{2ph}. \quad (11)$$

We characterize STIRAP, saSTIRAP and two-photon resonance processes within the limits of experimentally feasible parameters via quantum process tomography. We simulate a qutrit with $|0\rangle \rightarrow |1\rangle$ and $|1\rangle \rightarrow |2\rangle$ transition frequencies $\omega_{01}/2\pi = 5.27$ GHz and $\omega_{12}/2\pi = 4.82$ GHz respectively. The STIRAP and saSTIRAP drives consist of overlapping Gaussian pulses with maximum amplitudes $\bar{\Omega}_{01}/2\pi = \bar{\Omega}_{12}/2\pi = 45$ MHz and standard deviation, $\sigma = 35$ ns. The relative separation between these Gaussian pulses is given by $t_s = -0.8 \times \sigma$. We consider a qutrit initialized in nine different initial states, which are then evolved from $t_i = -182$ ns to $t_f = 140$ ns with $T = t_f - t_i$ in 1800 time steps. The frequencies of the Gaussian pulses are taken to be same as the respective qutrit transition frequencies.

We also perform quantum process tomography of STIRAP and saSTIRAP in the presence of decoherence. The evolution of the system is governed by the Lindblad master equation, $\dot{\rho} = -i/\hbar[H, \rho] + \mathcal{L}[\rho]$, where $\mathcal{L}[\rho] = \Gamma_{21}\rho_{22}(|1\rangle\langle 1| - |2\rangle\langle 2|) + \Gamma_{10}\rho_{11}(|0\rangle\langle 0| - |1\rangle\langle 1|) - \sum_{j,k \in \{0,1,2\}, j \neq k} \gamma_{jk}\rho_{jk}|j\rangle\langle k|$ is the Lindblad qutrit superoperator [30]

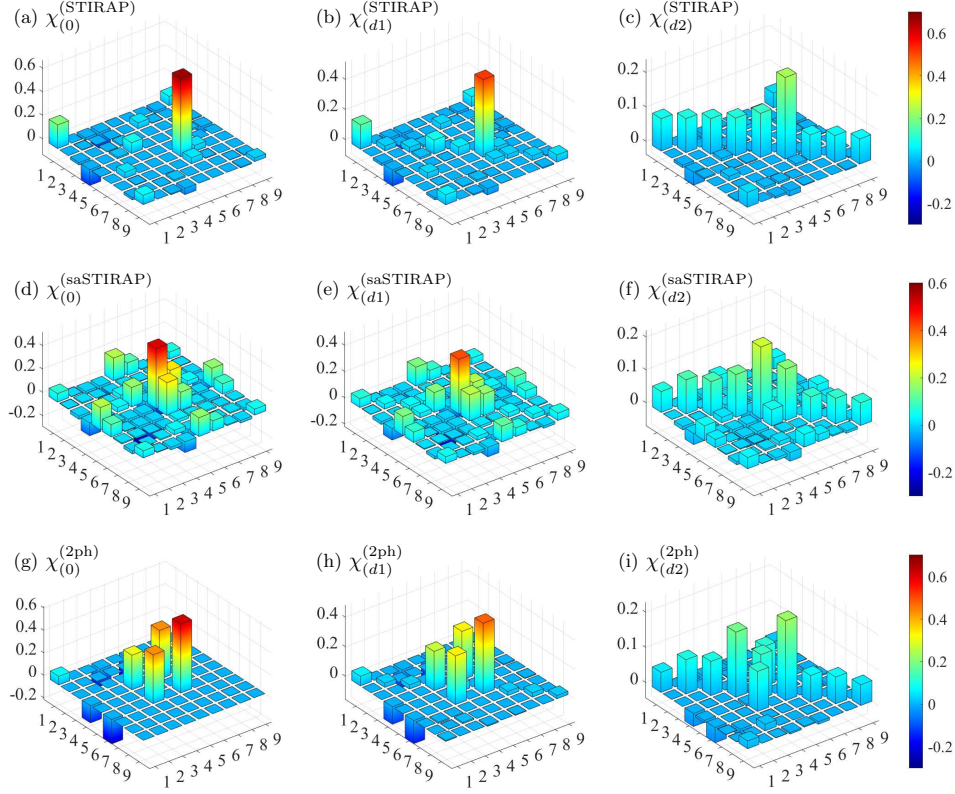


FIGURE 1. The process matrices for (a,b,c) STIRAP, (d,e,f) saSTIRAP, (g,h,i) two-photon processes are represented without decoherence, and with two different sets of decoherence parameters labelled by ($d1$) and ($d2$). Labels 1 – 9 along the x and y axes correspond to the set of single-qubit bases in the operator space, where label 1 corresponds to the identity operator (\mathbb{I}) and labels 2 – 9 stand for the Gell Mann matrices $\Lambda_1 - \Lambda_8$ respectively. The colorbars for sub figures in each row are shown at the right of that row.

with decoherence rates $\gamma_{10} = \Gamma_{10}/2 + \Gamma_{10}^\phi$, $\gamma_{20} = \Gamma_{21}/2 + \Gamma_{20}^\phi$, and $\gamma_{21} = (\Gamma_{10} + \Gamma_{21})/2 + \Gamma_{21}^\phi$. We simulate the evolution of this equation with two different sets of relaxation rates. The first set, labelled by ($d1$), has $\Gamma_{10} = 0.5$ MHz and $\Gamma_{21} = 0.71$ MHz and pure dephasing rates $\Gamma_{10}^\phi = 0.4$ MHz, $\Gamma_{21}^\phi = 0.56$ MHz, and $\Gamma_{20}^\phi = 0.96$ MHz, which correspond to realistic experimental values for transmons. The second set of decoherence parameters, labelled by ($d2$), simulate a situation with much higher decoherence. The parameters are $\Gamma_{10} = 2.5$ MHz, $\Gamma_{21} = 3.55$ MHz, $\Gamma_{10}^\phi = 2$ MHz, $\Gamma_{21}^\phi = 2.80$ MHz, and $\Gamma_{20}^\phi = 4.8$ MHz. The process matrices resulting from these simulations are shown in Figs. 1(a,b,c) for STIRAP with $H = H_0$ (Eq. 8), Figs. 1(d,e,f) for saSTIRAP governed by $H = H_{saSTIRAP}$ (Eq. 11) and Figs. 1(g,h,i) for the process resulting from two-photon resonance drive $H = H_{2ph}$ (Eq. 10). Figs. 1(a,d,e) do not involve decoherence, Figs. 1(b,e,h) result from the first set of typical experimental parameters determining decoherence, and Figs. 1(c,f,i) present the process matrices with much higher decoherence which has a higher tendency to enhance the elements at the diagonal.

Further, we obtain the fidelity of the process matrices obtained after decoherence $\chi_{(d)}$ with respect to the one without decoherence $\chi_{(0)}$ by employing the Uhlmann-Josza fidelity

$$\mathcal{F}_{0,d} = \left[\text{Tr} \sqrt{\sqrt{\chi_{(0)}} \chi_{(d)} \sqrt{\chi_{(0)}}} \right]^2.$$

Interestingly, comparing the process matrices for STIRAP and saSTIRAP, the saSTIRAP process seems to be relatively more robust against decoherence. This can be observed from the respective fidelities between $\chi_{(0)}$, $\chi_{(d1)}$ represented by $\mathcal{F}_{0,d1}$ and $\chi_{(0)}$, $\chi_{(d2)}$ represented by $\mathcal{F}_{0,d2}$ in Table I. As another measure for observing how different the processes are with and without decoherence, we calculate the trace distance between the respective process

	$\mathcal{F}_{0,d1}$	$\mathcal{F}_{0,d2}$	$\mathcal{D}_{0,d1}$	$\mathcal{D}_{0,d2}$	F_0	F_{d1}	F_{d2}
STIRAP	0.76	0.31	0.25	0.74	0.916	0.796	0.464
saSTIRAP	0.78	0.33	0.24	0.72	0.999	0.861	0.487
Two-photon process	0.78	0.33	0.24	0.72	0.888	0.770	0.446

TABLE I. Fidelity and trace distance values to compare different processes.

matrices by

$$\mathcal{D}_{0,d} = \sqrt{\text{Tr} [\chi_{(0)} - \chi_{(d)}]^2}.$$

Using this we obtain the trace distances: $\mathcal{D}_{0,d1}$ and $\mathcal{D}_{0,d2}$ between $\chi_{(0)}$, $\chi_{(d1)}$ and $\chi_{(0)}$, $\chi_{(d2)}$ respectively.

The fidelity $F_{0/d} = \langle 2|\rho_{0/d}|2\rangle$ with which the final state $\rho_{0/d}$ without/with decoherence matches with the theoretically expected state $|2\rangle$ is highest in case of saSTIRAP as shown in last three columns of Table I, where F_0 , F_{d1} , and F_{d2} represent the quantum state fidelities obtained in case of no decoherence, decohering environment with parameter set $d1$ and decoherence via parameter set $d2$ respectively. Thus saSTIRAP retains the precision of adiabatic STIRAP as well as the robustness of the two-photon drive.

DISCUSSION

The set of $d \times d$ -dimensional operators, which span the complete operator space of a d -dimensional quantum system, also serve as a very convenient basis for a process matrix. Here, in case of 3-dimensional quantum system, a set of eight Gell-Mann matrices alongwith the identity operator serve as the basis for the process matrix and as the generator of various unitary transformations. In the simplest case of one of the generators Λ_i as the Hamiltonian, there is a direct mapping of Λ_i to the $(i+1)^{\text{th}}$ diagonal element of the process matrix, while involvement of two or more generators give rise to the cross terms in the process matrix. Interestingly, the STIRAP Hamiltonian involves terms containing Λ_1 , Λ_2 , Λ_3 , Λ_6 , Λ_7 , Λ_8 , and \mathbb{I} , while it is designed to effectively obtain the $0-2$ transition, which in case of direct transition would correspond to Λ_4 and/or Λ_5 . Characterizing the STIRAP process clearly presents the dominated Λ_5 term in Fig. 1(a). Therefore, despite the STIRAP Hamiltonian being non-trivially hiding the $0-2$ coupling, the quantum process tomography correctly identifies the actual process. The saSTIRAP process matrix shown in Fig. 1(d) seem to have additional terms, due to the addition of the superadiabatic part of the Hamiltonian. The process matrices for STIRAP and saSTIRAP with decoherence are shown in Fig. 1(b,c,e,f) respectively. We notice that the involvement of decoherence tends to enhance the diagonal elements and suppress the cross terms depending upon the decoherence model in simulations or the actual decoherence observed in the physical systems.

ACKNOWLEDGMENTS

We acknowledge financial support from Foundational Questions Institute Fund (FQXi) via the Grant No. FQXi-IAF19-06, European Commission project QUARTET (grant agreement no. 862644, FET Open QUARTET), and from the Academy of Finland through the RADDESS programme (project no. 328193) and the ‘‘Finnish Center of Excellence in Quantum Technology QTF’’ (project 312296).

REFERENCES

1. M. A. Nielsen and I. L. Chuang, *Quantum Computation and Quantum Information*, quantum information, quantum computation, cryptography (Cambridge University Press, Cambridge UK, 2000).
2. A. Kandala, K. Temme, A. D. Córcoles, A. Mezzacapo, J. M. Chow, and J. M. Gambetta, ‘‘Error mitigation extends the computational reach of a noisy quantum processor,’’ *Nature* **567**, 491–495 (2019).
3. S. J. Devitt, ‘‘Performing quantum computing experiments in the cloud,’’ *Phys. Rev. A* **94**, 032329 (2016).
4. M. R. Perelshtein, A. I. Pakhomchik, A. A. Melnikov, A. A. Novikov, A. Glatz, G. S. Paraoanu, V. M. Vinokur, and G. B. Lesovik, ‘‘Advanced quantum supremacy using a hybrid algorithm for linear systems of equations,’’ arXiv:2003.12770 (2020).

5. G. García-Pérez, M. A. C. Rossi, and S. Maniscalco, "Ibm q experience as a versatile experimental testbed for simulating open quantum systems," *npj Quant. Inf.* **6**, 1 (2020).
6. A. Kandala, A. Mezzacapo, K. Temme, M. Takita, M. Brink, J. M. Chow, and J. M. Gambetta, "Hardware-efficient variational quantum eigensolver for small molecules and quantum magnets," *Nature* **549**, 242–246 (2017).
7. R. Harper and S. T. Flammia, "Fault-tolerant logical gates in the ibm quantum experience," *Phys. Rev. Lett.* **122**, 080504 (2019).
8. E. Huffman and A. Mizel, "Violation of noninvasive macrorealism by a superconducting qubit: Implementation of a leggett-garg test that addresses the clumsiness loophole," *Phys. Rev. A* **95**, 032131 (2017).
9. D. Alsina and J. I. Latorre, "Experimental test of mermin inequalities on a five-qubit quantum computer," *Phys. Rev. A* **94**, 012314 (2016).
10. G. Paraoanu, "Non-local parity measurements and the quantum pigeonhole effect," *Entropy* **20**, 606 (2018).
11. N. N. Hegade, A. Das, S. Seth, and P. K. Panigrahi, "Investigation of quantum pigeonhole effect in ibm quantum computer," arXiv:1904.12187.
12. A. Shukla, M. Sisodia, and A. Pathak, "Complete characterization of the directly implementable quantum gates used in the ibm quantum processors," *Physics Letters A* **384**, 126387 (2020).
13. I. L. Chuang and M. A. Nielsen, "Prescription for experimental determination of the dynamics of a quantum black box," *J. Mod. Opt.* **44**, 2455–2467 (1997).
14. M. Howard, J. Twamley, C. Wittmann, T. Gaebel, F. Jelezko, and J. Wrachtrup, "Quantum process tomography and linblad estimation of a solid-state qubit," *New Journal of Physics* **8**, 33–33 (2006).
15. R. C. Bialczak, M. Ansmann, M. Hofheinz, E. Lucero, M. Neeley, A. D. O'Connell, D. Sank, H. Wang, J. Wenner, M. Steffen, A. N. Cleland, and J. M. Martinis, "Quantum process tomography of a universal entangling gate implemented with josephson phase qubits," *Nature Physics* **6**, 409–413 (2010).
16. A. M. Palmieri, E. Kovlakov, F. Bianchi, D. Yudin, S. Straupe, J. D. Biamonte, and S. Kulik, "Experimental neural network enhanced quantum tomography," *npj Quantum Information* **6** (2020), 10.1038/s41534-020-0248-6.
17. A. Shukla and T. S. Mahesh, "Single-scan quantum process tomography," *Phys. Rev. A* **90**, 052301 (2014).
18. A. Gaikwad, D. Rehal, A. Singh, Arvind, and K. Dorai, "Experimental demonstration of selective quantum process tomography on an nmr quantum information processor," *Phys. Rev. A* **97**, 022311 (2018).
19. A. Bendersky, F. Pastawski, and J. P. Paz, "Selective and efficient estimation of parameters for quantum process tomography," *Phys. Rev. Lett.* **100**, 190403 (2008).
20. L. C. G. Govia, G. J. Ribeill, D. Ristè, M. Ware, and H. Krovi, "Bootstrapping quantum process tomography via a perturbative ansatz," *Nat. Commns.* **11**, 1084 (2020).
21. B. P. Lanyon, M. Barbieri, M. P. Almeida, T. Jennewein, T. C. Ralph, K. J. Resch, G. J. Pryde, J. L. O'Brien, A. Gilchrist, and A. G. White, "Simplifying quantum logic using higher-dimensional hilbert spaces," *Nat Phys* **5**, 134–140 (2009).
22. G. S. Paraoanu, "Recent progress in quantum simulation using superconducting circuits," *J. Low Temp. Phys.* **175**, 633–654 (2014).
23. J. Q. You and F. Nori, "Atomic physics and quantum optics usingsuperconducting circuits," *Nature* **474**, 589 (2011).
24. H.-S. Chang, Y. P. Zhong, A. Bienfait, M.-H. Chou, C. R. Conner, E. Dumur, G. Grebel, G. Peairs, R. G. Povey, K. J. Satzinger, and A. N. Cleland, "Remote entanglement via adiabatic passage using a tunably-dissipative quantum communication system," arXiv:2005.12334v1 (2020).
25. A. R. Shlyakhov, V. V. Zemlyanov, M. V. Suslov, A. V. Lebedev, G. S. Paraoanu, G. B. Lesovik, and G. Blatter, "Quantum metrology with a transmon qutrit," *Physical Review A* **97** (2018), 10.1103/physreva.97.022115.
26. S. Danilin, A. V. Lebedev, A. Vepsäläinen, G. B. Lesovik, G. Blatter, and G. S. Paraoanu, "Quantum-enhanced magnetometry by phase estimation algorithms with a single artificial atom," *npj Quantum Information* **4** (2018), 10.1038/s41534-018-0078-y.
27. M. S. Blok, V. V. Ramasesh, T. Schuster, K. O'Brien, J. M. Kreikebaum, D. Dahlen, A. Morvan, N. Y. Yoshida, B. amd Yao, and S. I., "Quantum information scrambling in a superconducting qutrit processor," arXiv:2003.03307 (2020).
28. G. Falci, A. Ridolfo, P. G. Di Stefano, and E. Paladino, "Ultrastrong coupling probed by coherent population transfer," *Scientific Reports* , 9249 (2019).
29. K. Bergmann, H.-C. Nägerl, C. Panda, G. Gabrielse, E. Miloglyadov, M. Quack, G. Seyfang, G. Wichmann, S. Ospelkaus, A. Kuhn, S. Longhi, A. Szameit, P. Pirro, B. Hillebrands, X.-F. Zhu, J. Zhu, M. Drewsen, W. K. Hensinger, S. Weidt, T. Halfmann, H.-L. Wang, G. S. Paraoanu, N. V. Vitanov, J. Mompert, T. Busch, T. J. Barnum, D. D. Grimes, R. W. Field, M. G. Raizen, E. Narevicius, M. Auzinsh, D. Budker, A. Pálffy, and C. H. Keitel, "Roadmap on STIRAP applications," *J. Phys. B* **52**, 202001 (2019).
30. K. S. Kumar, A. Vepsäläinen, S. Danilin, and G. S. Paraoanu, "Stimulated raman adiabatic passage in a three-level superconducting circuit," *Nat. Commun.* **7** (2016).
31. E. Torrontegui, S. Ibáñez, S. Martínez-Garaot, M. Modugno, A. del Campo, D. Guéry-Odelin, A. Ruschhaupt, X. Chen, and J. G. Muga, "Chapter 2 - shortcuts to adiabaticity," in *Advances in Atomic, Molecular, and Optical Physics*, Advances In Atomic, Molecular, and Optical Physics, Vol. 62, edited by P. R. B. Ennio Arimondo and C. C. Lin (Academic Press, 2013) pp. 117 – 169.
32. A. Vepsäläinen, S. Danilin, and G. S. Paraoanu, "Superadiabatic population transfer in a three-level superconducting circuit," *Sci. Adv.* **5** (2019).
33. A. Vepsäläinen, S. Danilin, and G. S. Paraoanu, "Optimal superadiabatic population transfer and gates by dynamical phase corrections," *Quantum Sci. Technol.* **3**, 024006 (2018).
34. A. Vepsäläinen, S. Danilin, E. Paladino, G. Falci, and G. S. Paraoanu, "Quantum control in qutrit systems using hybrid rabi-stirap pulses," *Photonics* **3** (2016), 10.3390/photonics3040062.
35. S. Dogra, A. Vepsäläinen, and G. S. Paraoanu, "Majorana representation of adiabatic and superadiabatic processes in three-level systems," *Phys. Rev. Research* **2**, 043079 (2020).
36. K. Kraus, "General state changes in quantum theory," *Annals of Physics* **64**, 311–335 (1971).
37. J. Stolze and D. Suter, *Quantum Computing: A Short Course from Theory to Experiment* (John Wiley & Sons, 2004).
38. G. Falci, P. G. Di Stefano, A. Ridolfo, A. D'Arrigo, G. S. Paraoanu, and E. Paladino, "Advances in quantum control of three-level superconducting circuit architectures," *Fortschritte der Phys.* **65**, 1600077 (2017).
39. A. Vepsäläinen, S. Danilin, and G. S. Paraoanu, "Simulating spin chains using a superconducting circuit: Gauge invariance, superadiabatic transport, and broken time-reversal symmetry," *Adv. Quantum Technol.* **3**, 1900121 (2020).